Collagen-based cell migration models in vitro and in vivo

Katarina Wolf[a], **Stephanie Alexander**[b], **Vivien Schacht**[c], **Lisa M. Coussens**[d], **Ulrich von Andrian**[e], **Jacco van Rheenen**[f], **Elena Deryugina**[g], and **Peter Friedl**[a,b]

Stephanie Alexander: StephanieAlexander@gmx.de; Vivien Schacht: vivien.schacht@uniklinik-freiburg.de; Lisa M. Coussens: Lisa.Coussens@ucsf.edu; Ulrich von Andrian: uva@idi.harvard.edu; Jacco van Rheenen: j.vanrheenen@hubrecht.eu; Elena Deryugina: deryugin@scripps.edu; Peter Friedl: p.friedl@ncmls.ru.nl

[a]Department of Cell Biology, Nijmegen Center for Molecular Life Science, Radboud University Nijmegen, P.O. Box 9101, 6500 HB Nijmegen, The Netherlands [b]Rudolf Virchow Center, DFG Research Center for Experimental Biomedicine and Department of Dermatology, University of Würzburg, Josef-Schneider-Str. 2, 97980 Würzburg, Germany [c]Cutaneous Biology Research Center, Massachusetts General Hospital and Harvard Medical School, 13th Street Charlestown, Boston, Massachusetts 02129, USA [d]Dept of Pathology, University of California, 513 Parnassus Ave., San Francisco, CA 94143, USA [e]Center for Blood Research, Harvard Medical School, 200 Longwood Avenue, Boston, MA 02115, USA [f]Hubrecht Institute-KNAW and University Medical Center Utrecht, Uppsalalaan 8, 3584CT Utrecht, The Netherlands [g]Department of Cell Biology, The Scripps Research Institute, 10550 North Torrey Pines Road, La Jolla, CA 92037, USA

Abstract

Fibrillar collagen is the most abundant extracellular matrix (ECM) constituent which maintains the structure of most interstitial tissues and organs, including skin, gut, and breast. Density and spatial alignment of the three-dimensional (3D) collagen architecture define mechanical tissue properties, i.e. stiffness and porosity, which guide or oppose cell migration and positioning in different contexts, such as morphogenesis, regeneration, immune response, and cancer progression. To reproduce interstitial cell movement in vitro with high in vivo fidelity, 3D collagen lattices are being reconstituted from extracted collagen monomers, resulting in the reassembly of a fibrillar meshwork of defined porosity and stiffness. With a focus on tumor invasion studies, we here evaluate different in vitro collagen-based cell invasion models, employing either pepsinized or un-pepsinized collagen extracts, and compare their structure to connective tissue in vivo, including mouse dermis and mammary gland, chick chorioallantoic membrane (CAM), and human dermis. Using confocal reflection and two-photon-excited second harmonic generation (SHG) microscopy, we here show that, depending on the collagen source, in vitro models yield homogeneous fibrillar texture with variable pore sizes, whereas all in vivo scaffolds comprise a range from low- to high-density fibrillar networks and heterogeneous pore sizes within the same tissue. Future in-depth comparison of structure and physical properties between 3D ECM-based models in vitro and in vivo are mandatory to better understand the mechanisms and limits of interstitial cell movements in distinct tissue environments.

*corresponding author: Katarina Wolf, Department of Cell Biology (283), NCMLS, Radboud University Nijmegen Medical Centre, P.O. Box 9101, 6500 HB Nijmegen, The Netherlands Tel: +31-24 3667377, Fax: +31-24 3615317; k.wolf@ncmls.ru.nl.
Present address: Department of Dermatology, University Medical Center Freiburg, Haupststrasse 7, 79104 Freiburg, Germany
Present address: Dept. of Pathology, Harvard Medical School, 77 Ave. Louis Pasteur, Boston, MA 02115, USA

Keywords

cancer cell invasion models; connective tissue geometry; physical collagen spacing; second harmonic generation microscopy

1. Introduction

In vertebrates, the ECM comprises at least two distinct types of scaffolds. Whereas basement membranes form a dense, flat protein meshwork underlying and anchoring epithelial and endothelial cells, interstitial connective tissues consist of a 3D protein meshwork of heterogeneous texture and composition. The main ECM component of interstitial tissues is fibrillar type I collagen that forms up to 90% protein content of connective tissues. The physical stability of connective tissues is mostly mediated by collagen fibrils, which are mechanically stable and provide a scaffold to which other ECM proteins such as fibronectin and gylcosaminoglycans connect.

After fibroblast-mediated synthesis of procollagen molecules, fibrillogenesis is initiated by the cleavage of N- and C-terminal propeptides from monomeric collagen, followed by the spontaneous collagen self-assembly into fibrils (Fig. 1A). Fibrils then receive slow secondary modification by stromal cell-derived lysyl oxidase which generates aldehyde groups at telopeptide-located lysyl or hydroxylysyl-residues that then spontaneously form aldimide (Schiff-base) cross-links with amino groups from a neighbouring collagen monomer [1,2]. This chemical modification leads to the formation of collagen fibrils and bundled fibres of enhanced mechanical stability [3].

Depending on further tissue-specific modifications and functions, such as protective or tensile stress-bearing tasks, collagen fibres are cross-linked to different extent and organized into quite heterogeneous structures. Interstitial connective tissue below epithelia contain porous but heterogeneously textured collagen networks, including thick bundles alternating with loosely organized thin fibres hosting blood and lymph vessels, and additional ECM components such as elastic fibres and fibronectin. Often these upper loose zones are connected to dense connective tissue and fat tissue. This basic organization is preserved in dermis, interstitial tissue of the gut and most parenchymatous organs. Collagen-rich ECM undergoes life-long remodeling and re-shaping by tissue cells such as fibroblasts that create adhesion receptor-mediated tension on ECM and physiologic slow proteolytic matrix turnover, a process that may become enhanced during wound healing or disease [4–7]. Interstitial ECM, on the other hand, influences cellular functions, besides acting as a major reservoir of releasable growth factors and peptide mediators, by physical characteristics, such as by fibre thickness, orientation, density, stiffness, or pore size between fibres [8–11]. These tissue structure-imposed changes on cell function are mediated by at least two distinct but interdependent mechanisms: (i) by mechanosensor-mediated and additional signaling cascades [12,13] and (ii) by guidance and confinement, respectively, of the cell body resulting in a shape adaptation in order to move [14,15]. Dimensionality as an additional aspect of tissue geometry influences cell-matrix interaction and consecutive movement which may take place along a single fibre (1D migration), across a sheet-like surface (2D movement), or through a spatially complex meshwork of fibrils (3D migration) [9,11,16–18]. Whereas 1D and

2D models provide important insights into the organization of molecular machineries underlying cell adhesion and migration, 3D migration models are instrumental in modeling cell dynamics with high fidelity to in vivo behavior [19]. In this review, we evaluate different 3D collagen-based models in vitro and in vivo, with a focus on the comparison of physical structure and spacing characteristics of collagen for the study of tumor cell movement.

2. Methods to visualize the 3D architecture of fibrillar collagens

The detection of fibrillar collagen only or within tissues can be achieved by several approaches that are based on distinct physicochemical parameters, using either dried processed or hydrated native samples. Fixed and chemically processed fibrillar collagens are traditionally assessed either in histological sections, transmission or scanning electron microscopy (SEM), revealing collagen organization and, particularly using SEM, additional contrast-producing solid structures [20]. Whereas the fibre geometry is preserved to high degree, these approaches do not allow the three-dimensional reconstruction of collagen architecture with sufficient fidelity, due to structural changes introduced by sample slicing, shrinkage artifacts and collapse. In contrast, the native 3D fibrillar collagen organization in hydrated state can be directly visualized by confocal reflection (*syn.* backscatter) microscopy [21] or two-photon-excited SHG microscopy [22,23]. Therefore, the latter two approaches provide more exact spacing information quantifiable by manual and automated image analysis approaches and computation [21,24].

2.1. Confocal reflection microscopy

For confocal reflection, light is introduced into the sample and the signal reflected by solid-state structures is detected in backward direction, thus any laser wavelength and sufficiently sensitive detection system will support this approach. Reflection of light occurs at interfaces between materials with different refractive indices, such as glass-water, collagen fibre-water, or cell membrane-water transitions, thus it is intrinsically non-specific and even cannot be distinguished from autofluorescence. However, it represents a powerful approach for high-contrast imaging of fibrillar scaffolds and (often fluorescently labelled) cells therein [18,21,25].

2.2. SHG

For the detection of fibrillar collagen structures within connective tissue in vivo, SHG is the method of choice. It is often visualized in conjunction with additional structures, such as striated muscles, elastic fibres and other cell and tissue components by specific SHG and autofluorescence signals [23,26]. The basic physical principle of SHG consists in the frequency-doubling of light by crystal-like repetitive but non-centrosymmetric structures, particularly polymers of helical proteins.

As technical setup, SHG requires a femto- or picosecond-pulsed high-power laser and photomultiplier-based detection in either forward or backward direction [23]. SHG of collagen is achieved by several wave-lengths between 800 and 1300 nm [23,27,28], and P. Friedl, unpublished observation. Because collagen SHG emission is exactly half the introduced wave-length, it can be spectrally quite precisely separated from other emission signals such as autoflorescence by beam splitters and dichroitic mirrors. SHG occurs only in the focal

plane providing sufficiently high photon density and, similar to two-photon-excited fluorescence microscopy, represents an inherently confocal approach allowing 3D reconstruction from z-slices. Consequently, the reconstruction of 3D specimens requires computerized z-positioning of sample stage or objective. For the in vivo imaging of mostly low transparent samples, SHG is commonly detected in backward direction using high-resolution long working-distance objectives of N.A.   0.95 (usually 20 × magnification). A key advantage of SHG is its compatibility with simultaneous detection of other light signals, including autofluorescence and fluorescence; its specific detection of collagen next to additional tissue structures; and its deep tissue penetration of relatively loose connective tissue structures. As main disadvantages, SHG is a polarization- and therefore angle-dependent process, that may generate higher signal intensity for some fibers and and lower signal for others; it further requires relatively high laser power with potential secondary damage to cells and tissue structures [23]; and its emission signal fades relatively fast in dense tissue specimens. All together, SHG represents an ideal method for detecting fibrillar collagen geometries within native/live connective tissues without the need for extrinsic labelling and sample processing.

3. Tissue structures of collagen-based ECM models

To study interstitial cell migration and invasion in vitro and in vivo, a number of collagen-based ECM models have been established [27,29–36]. These models are suited to examine distinct aspects of cell movement in a tissue-like environment, however, due to tissue source and geometry, vary in their basic structural properties. In vitro models consist of either de novo assembled fibres from extracted monomeric collagen that originate from different species, such as cow, calf, mouse, or rat. Alternatively, in vitro scaffolds stem from ex vivo collagen-rich connective tissues, including human native fresh skin, de-epidermized dermis (DED), and soft tissue substitutes, such as AlloDerm or Dermamatrix [37]. In vivo interstitial tissue models suited for intravital microscopy are available from several species and for almost every tissue type. We here evaluate 1) in vitro reconstituted 3D collagen lattices with 2) in vivo connective tissues of mouse or chicken origin, including mouse cremaster, skull dermis, dorsal skin and mammary gland, and the chicken CAM, and 3) ex vivo human dermis, and 4) directly compare their collagen structures.

3.1. 3D in vitro collagen models

3D fibrillar ECM models involve a discontinuous fibrillar substrate structure providing both an adhesion substrate as well as a steric barrier for moving cells, similar to collagen-rich interstitial tissues in vivo. Early in vitro research on cell behaviour within 3D reconstituted collagen-based ECM matrices employed processed rat tail collagen [38,39]. A number of variations have been developed, inlcuding supplementation with additional ECM components (e.g. fibrin, fibronectin, vitronectin, hyaloronic acid or basement membrane components) and stromal components (e.g. fibroblasts, vessel structures) or mounting on preparated animal connective tissues in vivo [25,31,40–43](P. Friedl, unpublished). The most popular are commercially available preparations of collagens extracted from rodent tails or bovine dermis. The collagen extraction process consists of several purification steps, such as raw material preparation, acid extration and optional pepsin treatment for solubilization,

filtration, purification by salt fractionation and/or column chromatography, and sterilization. Acid treatment (low molar acetic or hydrochloric acid) breaks collagen into monomers, which is sufficient for collagens with low-level covalent cross-links, characteristic of rat or mouse tail collagens. By contrast, more extensively cross-linked collagens, e.g. from bovine or huma dermis, require an additional pepsin treatment to cleave off cross-link mediating telopeptides. To initiate re-assembly of extracted collagen monomers from acidic solution, the pH is raised by basic solvents (usually containing bicarbonate or hydroxide ions). As pepsin treatment removes most of the assembly-initiating telopeptide sites, neutralized pepsinized collagen self-assembles into multimeric fibrils at delayed speed, compared to non-pepsinized collagen preparations [44](K. Wolf, unpublished observation). Consistent with delayed assembly, pepsin-digested collagens polymerize into more sparse lattices of longer fibrils between intersections resulting in larger pores with diameters of 3–5 μm, whereas telopeptide-containing collagens of the same protein content form shorter fibrils, smaller pores (ca. 1–2 μm diameter), and yield higher fibre density due to rapid initiation of fibre assembly (Fig. 1A). Because the collagen content is equal, variations in fibrillar density most likely result from different fibre diameters (K. Wolf, unpublished). Accordingly, whether treated or non-treated with pepsin, collagens from the same mouse tail source assemble into respectively loose or dense fibrillar networks (Fig. 1B). Further variables that influence collagen pore sizes are summarized in Table 1. Thus, both collagen type and the polymerization conditions have considerable influence on scaffold structure and porosity after in vitro reconstitution, and likely secondary impacts on cell morphology and behaviour including migration efficiency. For comparison, the size and shape of several cell types in polarized, hence migrating state are shown here, including small T lymphocytes, larger dendritic cells and large mesenchymal cells, such as fibroblasts or tumor cells (Fig. 1C). Thus, these different cellular dimensions need to be viewed in context of tissue gaps and spaces [45], (K. Wolf, manuscript in preparation). How such structural variability of in vitro collagen models reflects the topography of connective tissues in vivo, or regions therein, is unclear.

3.2. Interstitial in vivo animal models

To address how the structure of in vitro lattices corresponds to interstitial tissue in vivo, in vitro reconstituted 3D collagen has been compared to selected connective tissues from mouse or chicken embryo by SHG microscopy. An ever increasing number of experimental animal models has been developed for the examination of microvasular structures, cell dynamics, or tumor metastasis in mouse, rats, rabbit, hamster and chick embryo connective tissues, including ear, mesenterium, cremaster muscle, skull, back skin, and the CAM, using intravital microscopy [46–53]. More recently developed combinations of fluorescence and SHG microscopy are particularly suited to evaluate cell morphology and movement in relation to connective tissue spacing in the living animal [22,23,26–28,54,55]. The connective tissues from different sources contain fibrillar collagen networks of very heterogeneous architecture, consisting of loose areas with gaps and clefts of various sizes that are bordered by denser regions of thick collagen bundles aligned in parallel in the absence of obvious gaps and spaces (Figs. 2 and 3; see details below). For example, the collagen-rich periosteum of the mouse femur contains thick collagen bundles in parallel organization with clefts measuring 10 μm or less in width harbouring osteoclast precursors [26]. In the mouse

dermis or interstitial tissue of the mouse mammary gland, fibrillar collagen comprises spaces and gap diameters of less than 5 μm to more than 20 μm, allowing efficient tumor cell invasion [27,55,56].

3.2.1. Mouse connective tissue—We here assess mouse connective tissue regions often used for intravital microscopy, including mesenterium, cremaster muscle, mouse skull dermis of the frontoparietal scalp, mouse back dermis, and connective tissue of the mammary fat pad. The *mesenterium* displays a highly vascularized, thin connective tissue membrane providing blood supply to the gut system, which has been used preferably from rats or rabbits to study microvessel dynamics and leukocyte extravasation [57]. The mesenterial membrane consists of a dense sheet of collagen fibres organized in parallel which is only several μm thick, and thus represents a very thin 3D in vivo model (K.Wolf, unpublished data). The *cremaster* muscle holding and regulating the vicinity of the testes towards the abdomen is suitable and accessible for imaging of leukocyte migration. It consists of 1–2 layers of striated muscle fibres longitudinally organized, and parallel blood vessels that highly populate the cremaster muscle[49]. The central muscle layer contains interwoven losely organized collagen fibres and is laterally bordered by thick sheets of collagen fibres of 30 to 50 μm in depth and mostly parallel order, with gap diameters often exceeding 10–20 μm (Fig. 2A, asterisks). The *dermis above the frontoparietal mouse scalp* consists of several collagen-rich connective tissue layers underneath the epidermis with heterogeneous structure and density. Whereas upper regions comprise mostly loose connective tissue with substantial pores in between collagen fibres, deeper regions often exhibit compact, densely aligned collagen fibres with very small gaps, ranging in the tissue from approx. 3 to 10 μm in diameter (Fig. 2B). If monitored in the context with fluorescently labelled migrating tumor cells after injection into loose dermis regions, the cells readily displace with velocities of 1–5 μm per hour [27] and adapt their shape according to collagen fibre structure and pore diameter (K. Wolf and S. Alexander, unpublished observations). A similar macroporous fibrillar structure is visualized in the deep dermis of the mouse *back skin* nearby the deep dermal vascular plexus when monitored through a glass window of the dorsal skin fold chamber (DSFC). As compared to randomly organized dermis of the head region, both superficial (Fig. 2C) and deep regions of back skin dermis (Fig. 2D) comprise loose as well as more ordered regions with longitudinally oriented fiber bundles of heterogeneous density and interfibrillar spaces ranging between approx. 1 to 20 μm. In some regions, a high order of alignment is associated with adjacent tissue structures, such as hair follicles, apocrine and eccrine glands, and, as visualized in Fig. 2D, parallel muscle strands or blood vessels [34].

Finally, a *mammary tissue model* allows for the monitoring of connective tissue structures through a glass window [36,58]. In this model, a collageneous layer with interspersed blood vessels displays heterogeneously organized interconnected fibre strands and varying gap diameters ranging from below 1 μm up to 20 μm, similar to back dermis (Fig. 2E). Thus, depending on location and specific environment, collageneous connective tissue structures vary in their fibrillar density, orientation and spaces between fibres. These structural variations are likely associated with adjacent components, such as vessels, muscles, and fat cells.

3.2.2. Chick embryo CAM model—The CAM of the chick embryo is a traditional model for monitoring tumor dissemination, metastasis, and related angiogenesis [42,53,59]. The CAM displays a specialized, highly vascularized tissue that mediates gas exchange between the developing chick embryo and the atmosphere through the calcified eggshell. The fully developed CAM (day 10 of embryo development) consists of ectoderm, mesoderm, and endoderm, whereby the approximately 100 μm thick mesoderm comprises a loose collagen-rich connective tissue containing blood vessels and capillaries [59] (Fig. 3). The collagen meshwork is, in contrast to mouse connective tissue, of quite homogeneous order with gap diameters of around 10 μm. This model is often used for cancer cell invasion and metastasis studies [32,59,60], as it monitors invasion from the ectodermal layer across a basal membrane into very loose connective tissue. In summary, these in vivo animal models comprise heterogeneous collagen structures which range from randomly organized, very loose (CAM tissue, upper dermis) to dense architecture (thick collagen bundles in deep dermis) and, accordingly, exhibit heterogeneous pore diameters from sub- to almost supracellular spacing.

3.3. Human dermis models ex vivo

Fresh human dermis is the best-accessible connective tissue obtained as left-over from skin surgery (e.g. cosmetic surgery). Off-the shelf scaffolds comprise cadaveric human or porcine acellular dermal matrices (AllorDerm, Dermamatrix or Enduragen) which have been developed for skin grafting on acute and chronic wounds [37]. Native *human dermis* consists of densely packed thick long collagen bundles of 20 to 50 μm in diameter with interwoven loose collagen fibre meshworks, irrespective on whether fresh, processed or post-mortem processed dermis was analyzed (Fig. 4). The bundles display a tendency of alternating horizontal and perpendicular organization, often bordered by aligned elastic fibres, with heterogeneously configured pores of approx. 2 to 10 μm in diameter. Very similar to native human dermis, *DED,* which originates from abdominal skin [61] displays a network consisting of mostly densely packed collagen bundles interspersed with infrequent gaps and clefts similar to fresh dermis (Fig. 4B). Likewise, human *cadaveric dermal matrix* (AlloDerm) consists of compact fibre bundles with a high degree of parallel organization and adjacent elastic fibres but relatively rare longitudinal gaps and ECM tracks (Fig. 4C). Thus, compared to native hydrated dermis, processed acellular dermis displays an increased degree of compaction. The differences in fibre packing and resulting pore size between native and processed dermis may stem from variations between donors and tissue locations, as well as structural changes introduced by tissue processing. All three types of human dermis have been used to monitor vertical cancer invasion (P. Friedl, unpublished observation) [32,61]. Clearly, more systematic studies are needed to better map physical interstitial tissue properties that take into account donor variability including sex and age, tissue origins, and the effects of post-treatment procedures. Compared to interstitial murine and CAM tissue, human dermis shows a higher degree of organization but retains the alternation between loose and dense regions.

3.4. Comparison of fibre structures and resulting pore sizes in collagen-based models

Looking at all the introduced models in context, the main difference is that the structural complexity in vivo is incompletely represented by in vitro reconstituted collagen scaffolds.

In vitro collagen monomers assemble to homogeneous networks of rather equally sized pores that may mimic either loose or dense ECM, but not both in conjunction. The connective tissues examined here are heterogeneous in organization with interspersed low- and high density collagen regions resulting in variable gap diameters and clefts (Fig. 5A). To quantitatively compare the structure and spacing of such different in vitro and in vivo tissues, confocal reflection (for in vitro reconstituted collagen) and SHG (for in vivo tissues) were used and matrix pore sizes relative to known sizes and shapes of different cell types were analyzed by morphometric analysis, as described [21,23]. The quantification of collagen-free spaces from xy images showed model-specific variation. The median pore area of non-pepsinized and pepsinized collagen was approx. 2 μm^2 and 15 μm^2, respectively, with a total range from 1 to 40 μm^2 (Fig. 5B). Consistent with heterogeneity, in vivo connective tissues show an increased variation of collagen-free spaces, ranging from ca. 10 to 1000 μm^2 (Fig. 5B). Accordingly, the median distance between fibres which corresponds to pore diameters was 1,7 μm for non-pepsinized and 3,2 μm for pepsinized collagen with a total range from 1 to 5 μm, and, again, increased variation in connectives tissues range from ca. 1 to above 20 μm (Fig. 5C). Interestingly, the CAM model displays the greatest homogeneity compared to other connective tissues which comprise both, low- and high-density regions. In conclusion, compared to connective tissue models in vivo, 3D collagen-based in vitro models contain more homogeneous collagen structures with characteristic average pore sizes for each different preparation. Thus, in vitro gap diameters but not the overall architecture correspond to both, in vivo porosity, whereby pepsinized, but not non-pepsinized collagen lattices are of intermediate density between low and high density dermis in vivo, and suited to accommodate all cell bodies of leukocytic and non-leukocytic cells. Such knowledge on ECM structure and spacing should be taken into account for designing and refining in vitro and in vivo models for cell migration.

4. Tumor-associated changes in collagen-structure

In this review, we compared collagen structures in basic in vitro systems and connective tissue of healthy animals suitable as tumor cell invasion models which, in fact, neglects that during most disease processes the constitutve tissue structure may be strongly remodeled. During cancerous transformation, structural changes develop in the tumor-surrounding collageneous tissues that can be visualized by SHG microscopy [20,62,63]. In particular, the progression of palpable breast cancers including increased local invasion into surrounding connective tissues coincides with increase in local collagen concentration, rigidity, realignment of collagen fibres towards the tumor edge, most likely cross-linking, and the deposition of additional ECM components and ECM fragments. Such structural changes in the tumor-surrounding collagen are associated with increased collagen and lysyl oxidase production, an increased tension mediated by mechanoreceoptor-cytoskeletal linkages, and proteolytic matrix remodeling by the action of ECM-degrading proteases [11,12,20,63]. Thus, ECM architecture and associated cell function need to be viewed in the context of both, constitutive and diseased state.

5. Conclusions

The complex texture of collagen-rich connective tissue is created by substantial structural and spatial heterogeneities, including collagen density, cross-linked induced fibre bundling and thickness, fibre orientation into longitudinal bundles or more random networks, and resulting gaps and clefts between collagen fibres and bundles. These varying collagen patterns are obtained within the same tissue, different tissue regions of the same species, and between species. Based on these structural characteristics, connective tissue-derived collagen displays a dual function for cell movement as (i) guidance structure providing preformed tracks, and (ii) barrier by forming fibre networks with random gaps of subcellular size. As an important fact in the evaluation of cell migration models, this heterogeneity will determine the type of cell movement, such as 3D invasion through relatively small tissue gaps, migration along fibrillar guidance structures and paths of least resistance (contact guidance), or 2D migration on interstitial surfaces, such as thick collagen bundles [15,20,55].

Besides fibrillar collagen, other structural components impact the type, efficiency and direction of cell migration, including blood and lymph vessels, muscular strands, ducts, glands, and nerves. Thus, the connective tissue models reviewed here require more in-depth structural and chemical analysis to map also the composition of these guidance structures. Further, collagen-free solid areas need to be structurally analyzed for their content of additional solid components that cannot be captured by SHG microscopy. Lastly, all analyses would benefit from measurements of physical collagen properties, such as stiffness and ultrastructural surface properties of collagen bundle structures.

When comparing 3D in vitro and connective tissue collagen, in vitro collagen lattices reproduce with sufficient fidelity the structural characteristics of rather loose, network-like organized interstitial tissues, not however, cross-link matured packed interstitial tissue. In addition, in vitro lattices lack the structural heterogeneity of fiber calibres and pore sizes present in connective tissues. To experimentally mimic cell movement closer to the tissue geometry in vivo, 3D collagen models could be designed that resemble collagen characteristics in vivo as close as possible, by adapting fibre alignment, LOX-induced maturation and stiffness, or varying pore sizes. A promising strategy to increase the structural order of in vitro reconstituted 3D collagen lattices is the conditioning and secondary remodeling by stromal cells, such as fibroblasts, endothelial cells, or cancer cells themselves [11,31,64–66].

To take the impact of tissue physics on cell function into account, careful structural analysis should accompany molecular analysis of cell functions in 3D ECM. To date, systematic studies comparing the structure and function of rodent with human interstitial tissues are lacking. The here reviewed data comparing murine with human collagen structure of the dermis suggest, that the structural and physical parameters diverge, yet common principles of varying pore sizes in the range of several micrometers are retained. Likewise, spatial characteristics may vary depending on the collagen source for in vitro reconstituted collagen models. The knowledge about specific ECM spacing and density is further important for studies focussing on proteolytic ECM barrier removal and reorganization. To compare data

derived from different 3D collagen-based cell function models, it will therefore be important to map ECM structures of different models systematically.

Acknowledgments

Abbreviations

ECM	extracellular matrix
3D	three-dimensional
SHG	second harmonic generation
CAM	chorioallantoic membrane
DSFC	dorsal skin fold chamber
DED	de-epidermized dermis

References

1. Siegel RC. Biosynthesis of collagen crosslinks: increased activity of purified lysyl oxidase with reconstituted collagen fibrils. Proc Natl Acad Sci U S A. 1974; 71:4826–30. [PubMed: 4531019]

2. Sabeh F, Shimizu-Hirota R, Weiss SJ. Protease-dependent versus -independent cancer cell invasion programs: three-dimensional amoeboid movement revisited. J Cell Biol. 2009; 185:11–9. [PubMed: 19332889]

3. Elbjeirami WM, Yonter EO, Starcher BC, West JL. Enhancing mechanical properties of tissue-engineered constructs via lysyl oxidase crosslinking activity. J Biomed Mater Res A. 2003; 66:513–21. [PubMed: 12918034]

4. Paszek MJ, Zahir N, Johnson KR, Lakins JN, Rozenberg GI, Gefen A, et al. Tensional homeostasis and the malignant phenotype. Cancer Cell. 2005; 8:241–54. [PubMed: 16169468]

5. Daley WP, Peters SB, Larsen M. Extracellular matrix dynamics in development and regenerative medicine. J Cell Sci. 2008; 121:255–64. [PubMed: 18216330]

6. Stetler-Stevenson WG, Liotta LA, Kleiner DE Jr. Extracellular matrix 6: role of matrix metalloproteinases in tumor invasion and metastasis. Faseb J. 1993; 7:1434–41. [PubMed: 8262328]

7. Zhai Y, Hotary KB, Nan B, Bosch FX, Munoz N, Weiss SJ, et al. Expression of membrane type 1 matrix metalloproteinase is associated with cervical carcinoma progression and invasion. Cancer Res. 2005; 65:6543–50. [PubMed: 16061633]

8. Harley BA, Kim HD, Zaman MH, Yannas IV, Lauffenburger DA, Gibson LJ. Microarchitecture of three-dimensional scaffolds influences cell migration behavior via junction interactions. Biophys J. 2008; 95:4013–24. [PubMed: 18621811]

9. Poole K, Khairy K, Friedrichs J, Franz C, Cisneros DA, Howard J, et al. Molecular-scale topographic cues induce the orientation and directional movement of fibroblasts on two-dimensional collagen surfaces. J Mol Biol. 2005; 349:380–6. [PubMed: 15890202]

10. Grew JC, Ricci JL, Alexander H. Connective-tissue responses to defined biomaterial surfaces. II. Behavior of rat and mouse fibroblasts cultured on microgrooved substrates. J Biomed Mater Res A. 2008; 85:326–35. [PubMed: 17688289]

11. Wolf K, Wu YI, Liu Y, Geiger J, Tam E, Overall C, et al. Multi-step pericellular proteolysis controls the transition from individual to collective cancer cell invasion. Nat Cell Biol. 2007; 9:893–904. [PubMed: 17618273]

12. Butcher DT, Alliston T, Weaver VM. A tense situation: forcing tumour progression. Nat Rev Cancer. 2009; 9:108–22. [PubMed: 19165226]

13. Giannone G, Sheetz MP. Substrate rigidity and force define form through tyrosine phosphatase and kinase pathways. Trends Cell Biol. 2006; 16:213–23. [PubMed: 16529933]

14. Friedl P, Wolf K. Proteolytic and non-proteolytic migration of tumour cells and leucocytes. Biochem Soc Symp. 2003:277–85. [PubMed: 14587300]

15. Wolf K, Muller R, Borgmann S, Brocker EB, Friedl P. Amoeboid shape change and contact guidance: T-lymphocyte crawling through fibrillar collagen is independent of matrix remodeling by MMPs and other proteases. Blood. 2003; 102:3262–9. [PubMed: 12855577]

16. Doyle AD, Wang FW, Matsumoto K, Yamada KM. One-dimensional topography underlies three-dimensional fibrillar cell migration. J Cell Biol. 2009; 184:481–90. [PubMed: 19221195]

17. d'Ortho MP, Stanton H, Butler M, Atkinson SJ, Murphy G, et al. MT1-MMP on the cell surface causes focal degradation of gelatin films. FEBS Lett. 1998; 421:159–64. [PubMed: 9468298]

18. Kim A, Lakshman N, Petroll WM. Quantitative assessment of local collagen matrix remodeling in 3-D culture: the role of Rho kinase. Exp Cell Res. 2006; 312:3683–92. [PubMed: 16978606]

19. Friedl P, Bröcker E-B. The biology of cell locomotion within three-dimensional extracellular matrix. Cell Mol Life Sci. 2000; 57:41–64. [PubMed: 10949580]

20. Provenzano PP, Eliceiri KW, Campbell JM, Inman DR, White JG, Keely PJ. Collagen reorganization at the tumor-stromal interface facilitates local invasion. BMC Med. 2006; 4:38. [PubMed: 17190588]

21. Friedl P, Maaser K, Klein CE, Niggemann B, Krohne G, Zanker KS. Migration of highly aggressive MV3 melanoma cells in 3-dimensional collagen lattices results in local matrix reorganization and shedding of alpha2 and beta1 integrins and CD44. Cancer Res. 1997; 57:2061–70. [PubMed: 9158006]

22. Campagnola PJ, Millard AC, Terasaki M, Hoppe PE, Malone CJ, Mohler WA. Three-dimensional high-resolution second-harmonic generation imaging of endogenous structural proteins in biological tissues. Biophys J. 2002; 82:493–508. [PubMed: 11751336]

23. Friedl P, Wolf K, Harms G, von Andrian UH. Biological second and third harmonic generation microscopy. Curr Protoc Cell Biol. 2007; Chapter 4(Unit 4):15. [PubMed: 18228516]

24. Bayan C, Levitt JM, Miller E, Kaplan D, Georgakoudi I. Fully automated, quantitative, noninvasive assessment of collagen fiber content and organization in thick collagen gels. J Appl Physics. 2009; 105:102042-1–11.

25. Maaser K, Wolf K, Klein CE, Niggemann B, Zanker KS, Brocker EB, et al. Functional hierarchy of simultaneously expressed adhesion receptors: integrin alpha2beta1 but not CD44 mediates MV3 melanoma cell migration and matrix reorganization within three-dimensional hyaluronan-containing collagen matrices. Mol Biol Cell. 1999; 10:3067–79. [PubMed: 10512851]

26. Zipfel WR, Williams RM, Christie R, Nikitin AY, Hyman BT, Webb WW. Live tissue intrinsic emission microscopy using multiphoton-excited native fluorescence and second harmonic generation. Proc Natl Acad Sci U S A. 2003; 100:7075–80. [PubMed: 12756303]

27. Wolf K, Mazo I, Leung H, Engelke K, von Andrian UH, Deryugina EI, et al. Compensation mechanism in tumor cell migration: mesenchymal-amoeboid transition after blocking of pericellular proteolysis. J Cell Biol. 2003; 160:267–77. [PubMed: 12527751]

28. Andresen V, Alexander S, Heupel WM, Hirschberg M, Hoffman RM, Friedl P. Infrared multiphoton microscopy: subcellular-resolved deep tissue imaging. Curr Opin Biotechnol. 2009; 20:54–62. [PubMed: 19324541]

29. Ntayi C, Lorimier S, Berthier-Vergnes O, Hornebeck W, Bernard P. Cumulative influence of matrix metalloproteinase-1 and -2 in the migration of melanoma cells within three-dimensional type I collagen lattices. Exp Cell Res. 2001; 270:110–8. [PubMed: 11597133]

30. Carragher NO, Walker SM, Scott Carragher LA, Harris F, Sawyer TK, Brunton VG, et al. Calpain 2 and Src dependence distinguishes mesenchymal and amoeboid modes of tumour cell invasion: a link to integrin function. Oncogene. 2006; 25:5726–40. [PubMed: 16652152]

31. Gaggioli C, Hooper S, Hidalgo-Carcedo C, Grosse R, Marshall JF, Harrington K, et al. Fibroblast-led collective invasion of carcinoma cells with differing roles for RhoGTPases in leading and following cells. Nat Cell Biol. 2007; 9:1392–400. [PubMed: 18037882]

32. Sabeh F, Ota I, Holmbeck K, Birkedal-Hansen H, Soloway P, Balbin M, et al. Tumor cell traffic through the extracellular matrix is controlled by the membrane-anchored collagenase MT1-MMP. J Cell Biol. 2004; 167:769–81. [PubMed: 15557125]

33. Zijlstra A, Lewis J, Degryse B, Stuhlmann H, Quigley JP. The inhibition of tumor cell intravasation and subsequent metastasis via regulation of in vivo tumor cell motility by the tetraspanin CD151. Cancer Cell. 2008; 13:221–34. [PubMed: 18328426]

34. Alexander S, Koehl GE, Hirschberg M, Geissler EK, Friedl P. Dynamic imaging of cancer growth and invasion: a modified skin-fold chamber model. Histochem Cell Biol. 2008; 130:1147–54. [PubMed: 18987875]

35. Nelson CM, Vanduijn MM, Inman JL, Fletcher DA, Bissell MJ. Tissue geometry determines sites of mammary branching morphogenesis in organotypic cultures. Science. 2006; 314:298–300. [PubMed: 17038622]

36. Kedrin D, Gligorijevic B, Wyckoff J, Verkhusha VV, Condeelis J, Segall JE, et al. Intravital imaging of metastatic behavior through a mammary imaging window. Nat Methods. 2008; 5:1019–21. [PubMed: 18997781]

37. Gordley K, Cole P, Hicks J, Hollier L. A Comparative, long term assessment of soft tissue substitutes: AlloDerm, Enduragen, and Dermamatrix. J Plast Reconstr Aesthet Surg. 2009

38. Ehrmann RL, Gey GO. The growth of cells on a transparent gel of reconstituted rat-tail collagen. J Natl Cancer Inst. 1956; 16:1375–403. [PubMed: 13320119]

39. Elsdale T, Bard J. Collagen substrata for studies on cell behavior. J Cell Biol. 1972; 54:626–37. [PubMed: 4339818]

40. Clark RA, Lin F, Greiling D, An J, Couchman JR. Fibroblast invasive migration into fibronectin/fibrin gels requires a previously uncharacterized dermatan sulfate-CD44 proteoglycan. J Invest Dermatol. 2004; 122:266–77. [PubMed: 15009704]

41. Krause S, Maffini MV, Soto AM, Sonnenschein C. A novel 3D in vitro culture model to study stromal-epithelial interactions in the mammary gland. Tissue Eng Part C Methods. 2008; 14:261–71. [PubMed: 18694322]

42. Deryugina EI, Quigley JP. Chapter 2. Chick embryo chorioallantoic membrane models to quantify angiogenesis induced by inflammatory and tumor cells or purified effector molecules. Methods Enzymol. 2008; 444:21–41. [PubMed: 19007659]

43. Mueller MM, Fusenig NE. Friends or foes - bipolar effects of the tumour stroma in cancer. Nat Rev Cancer. 2004; 4:839–49. [PubMed: 15516957]

44. Helseth DL Jr, Veis A. Collagen self-assembly in vitro. Differentiating specific telopeptide-dependent interactions using selective enzyme modification and the addition of free amino telopeptide. J Biol Chem. 1981; 256:7118–28. [PubMed: 7251588]

45. Friedl P, Zanker KS, Bröcker E-B. Cell migration strategies in 3-D extracellular matrix: differences in morphology, cell matrix interactions, and integrin function. Microsc Res Tech. 1998; 43:369–78. [PubMed: 9858334]

46. Wood S Jr. Pathogenesis of metastasis formation observed in vivo in the rabbit ear chamber. AMA Arch Pathol. 1958; 66:550–68. [PubMed: 13582395]

47. Cliff WJ. The acute inflammatory reaction in the rabbit ear chamber with particular reference to the phenomenon of leukocytic migration. J Exp Med. 1966; 124:543–56. [PubMed: 5922284]

48. Baez S. An open cremaster muscle preparation for the study of blood vessels by in vivo microscopy. Microvasc Res. 1973; 5:384–94. [PubMed: 4709735]

49. Mempel TR, Moser C, Hutter J, Kuebler WM, Krombach F. Visualization of leukocyte transendothelial and interstitial migration using reflected light oblique transillumination in intravital video microscopy. J Vasc Res. 2003; 40:435–41. [PubMed: 14530600]

50. Mazo IB, Gutierrez-Ramos JC, Frenette PS, Hynes RO, Wagner DD, von Andrian UH. Hematopoietic progenitor cell rolling in bone marrow microvessels: parallel contributions by endothelial selectins and vascular cell adhesion molecule 1. J Exp Med. 1998; 188:465–74. [PubMed: 9687524]

51. Endrich B, Asaishi K, Gotz A, Messmer K. Technical report--a new chamber technique for microvascular studies in unanesthetized hamsters. Res Exp Med (Berl). 1980; 177:125–34. [PubMed: 7003665]

52. Asaishi K, Endrich B, Gotz A, Messmer K. Quantitative analysis of microvascular structure and function in the amelanotic melanoma A-Mel-3. Cancer Res. 1981; 41:1898–904. [PubMed: 7214358]

53. Armstrong PB, Quigley JP, Sidebottom E. Transepithelial invasion and intramesenchymal infiltration of the chick embryo chorioallantois by tumor cell lines. Cancer Res. 1982; 42:1826–37. [PubMed: 7066899]

54. Condeelis J, Segall JE. Intravital imaging of cell movement in tumours. Nat Rev Cancer. 2003; 3:921–30. [PubMed: 14737122]

55. Pinner S, Sahai E. Imaging amoeboid cancer cell motility in vivo. J Microsc. 2008; 231:441–5. [PubMed: 18754999]

56. Sidani M, Wyckoff J, Xue C, Segall JE, Condeelis J. Probing the microenvironment of mammary tumors using multiphoton microscopy. J Mammary Gland Biol Neoplasia. 2006; 11:151–63. [PubMed: 17106644]

57. Wakelin MW, Sanz MJ, Dewar A, Albelda SM, Larkin SW, Boughton-Smith N, et al. An anti-platelet-endothelial cell adhesion molecule-1 antibody inhibits leukocyte extravasation from mesenteric microvessels in vivo by blocking the passage through the basement membrane. J Exp Med. 1996; 184:229–39. [PubMed: 8691137]

58. Gligorijevic B, Kedrin D, Segall JE, Condeelis J, van Rheenen J. Dendra2 photoswitching through the Mammary Imaging Window. J Vis Exp. 2009:28.

59. Deryugina EI, Quigley JP. Chick embryo chorioallantoic membrane model systems to study and visualize human tumor cell metastasis. Histochem Cell Biol. 2008; 130:1119–30. [PubMed: 19005674]

60. Li XY, Ota I, Yana I, Sabeh F, Weiss SJ. Molecular dissection of the structural machinery underlying the tissue-invasive activity of membrane type-1 matrix metalloproteinase. Mol Biol Cell. 2008; 19:3221–33. [PubMed: 18495869]

61. van Kilsdonk JW, Wilting RH, Bergers M, van Muijen GN, Schalkwijk J, van Kempen LC, et al. Attenuation of melanoma invasion by a secreted variant of activated leukocyte cell adhesion molecule. Cancer Res. 2008; 68:3671–9. [PubMed: 18483249]

62. Brown E, McKee T, diTomaso E, Pluen A, Seed B, Boucher Y, Jain RK. Dynamic imaging of collagen and its modulation in tumors in vivo using second-harmonic generation. Nat Med. 2003; 9:796–800. [PubMed: 12754503]

63. Han X, Burke RM, Zettel ML, Tang P, Brown EB. Second harmonic properties of tumor collagen: determining the structural relationship between reactive stroma and healthy stroma. Opt Express. 2008; 16:1846–59. [PubMed: 18542263]

64. Bell SE, Mavila A, Salazar R, Bayless KJ, Kanagala S, Maxwell SA, et al. Differential gene expression during capillary morphogenesis in 3D collagen matrices: regulated expression of genes involved in basement membrane matrix assembly, cell cycle progression, cellular differentiation and G-protein signaling. J Cell Sci. 2001; 114:2755–73. [PubMed: 11683410]

65. Friedl P, Wolf K. Proteolytic interstitial cell migration: a five-step process. Cancer Metastasis Rev. 2009; 28:129–35. [PubMed: 19153672]

66. Maniotis AJ, Folberg R, Hess A, Seftor EA, Gardner LM, Pe'er J, et al. Vascular channel formation by human melanoma cells in vivo and in vitro: vasculogenic mimicry. Am J Pathol. 1999; 155:739–52. [PubMed: 10487832]

67. Raub CB, Unruh J, Suresh V, Krasieva T, Lindmo T, Gratton E, et al. Image correlation spectroscopy of multiphoton images correlates with collagen mechanical properties. Biophys J. 2008; 94:2361–73. [PubMed: 18065452]

68. Raub CB, Suresh V, Krasieva T, Lyubovitsky J, Mih JD, Putnam AJ, et al. Noninvasive assessment of collagen gel microstructure and mechanics using multiphoton microscopy. Biophys J. 2007; 92:2212–22. [PubMed: 17172303]

69. Gobeaux F, Mosser G, Anglo A, Panine P, Davidson P, Giraud-Guille MM, et al. Fibrillogenesis in dense collagen solutions: a physicochemical study. J Mol Biol. 2008; 376:1509–22. [PubMed: 18234220]
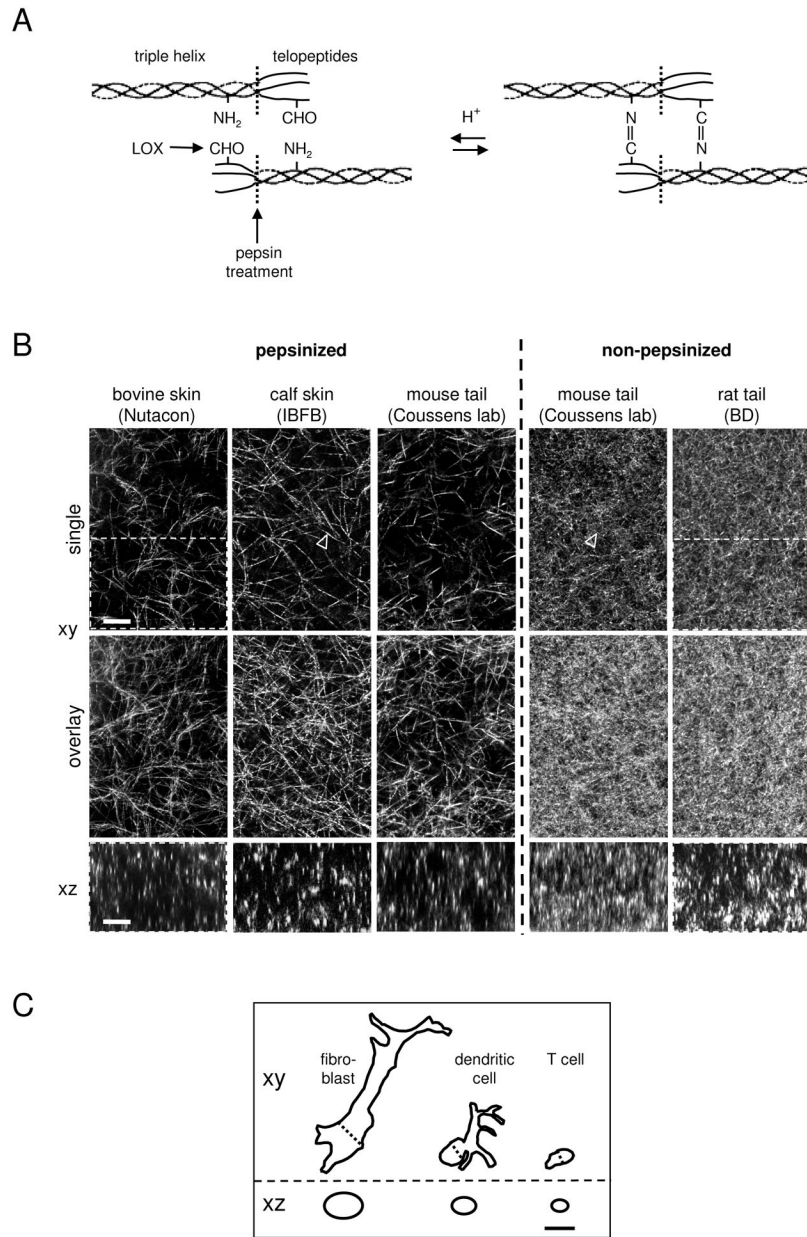
Figure 1.
Structure of 3D fibrillar collagen reconstituted in vitro from different collagen sources. (A) Structure of collagen monomers containing telopeptide and respective pepsin cleavage site in both, solublized (acidic) and multimeric state. Aldehyde (CHO) moities are generated by lysyl oxidase (LOX) spontaneously assembling into aldimine cross-links (adapted from [2]). (B) Polymerized networks of pepsinized (telopeptide-free) or non-pepzinized (telopeptide-containing) collagens from different sources and suppliers (bovine skin, Nutacon, Leiden, The Netherlands; calf skin, IBFB, Leipzig, Germany; mouse tail, Lisa Coussens lab, San Francisco, USA; rat tail, Becton Dickinson). For all matrices, a final collagen concentration of 1.7 mg/ml and standard polymerization procedures were used, as described ([11] and protocols provided by suppliers). Top row, single xy scan; middle row, overlay covering 8

μm in depth; bottom row, single xz scan. Because of the matrix dimensions, collagen fibre orientation is mostly in parallel to the upper and lower cover slips, leading to longitudinal reflection in xy scans and dot-like cross-section like signal in xz scans. Arrowheads: single collagen fibres. Marked areas refer to Fig. 5. (C) Outlines of typical migrating cells in horizontal and vertical dimension in 1:1 ratio to collagen structures depicted in (A). The outline of the mesenchymal cell (ca. $50\times10\times10$ μm and 75 μm^2 area in xz) is similar to many tumor cells from epithelial or mesenchymal origin, whereas trafficking leukocytes are smaller (dendritic cell, ca. $15\times7\times7$ μm, 35 μm^2 area in xz; T cell, ca. $10\times4\times5$, 15 μm^2 area in xz)[45]. Bars, 10 μm.
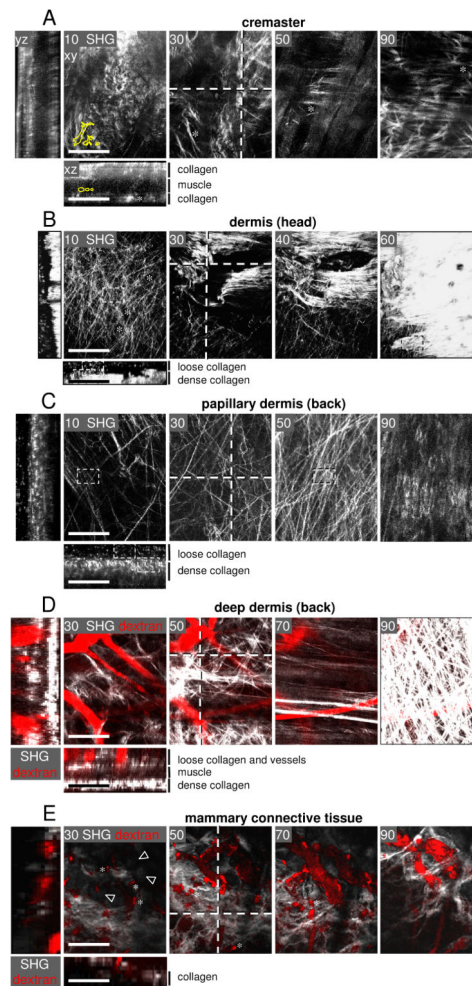
Fig. 2.
Collagen spacing of 3D mouse connective tissue models in vivo. Intravital two-photon microscopy was performed in connective tissues of anaesthetized mice from different locations using different experimental procedures (in brackets): (A) cremaster muscle (open surgery) [48,49], (B) skull (frontoparietal scalp; open surgery) [27,50], (C, D) back skin dermis (DSFC) [34,51], and (E) mammary fat pad (mammary imaging window)[36,58]. (A) Mouse cremaster model. Asterisks, SHG-negative gaps. B) Mouse dermis of the head region. Asterisks indicate SHG-negative spaces presumably filled with vessel tubes, based on roundish morphology. (C) Mouse dermis of the back skin in papillary (superficial) and (D) deep reticular dermis. (E) Collagen-rich region of the mammary fat pad. (D, E) Fluorescent dextran (red) was used to counterstain perfused blood vessels and (after uptake) tissue-resident macrophages (asterisks) [34,36]. (E) Arrowheads, fat cells. (A–E) Xy images represent individual planes from z-stacks at different imaging depth (numbers in images, μm of depth). Dotted lines, location of xz and yz images shown in the left and lower panels, using the ImageJ software (version 1.41o). Small dotted rectangles in (B, C) show the sections used for quantification in Fig. 5. In some images, cell outlines from Fig. 1C are displayed in 1:1 ratio. Bars, 100 μm.
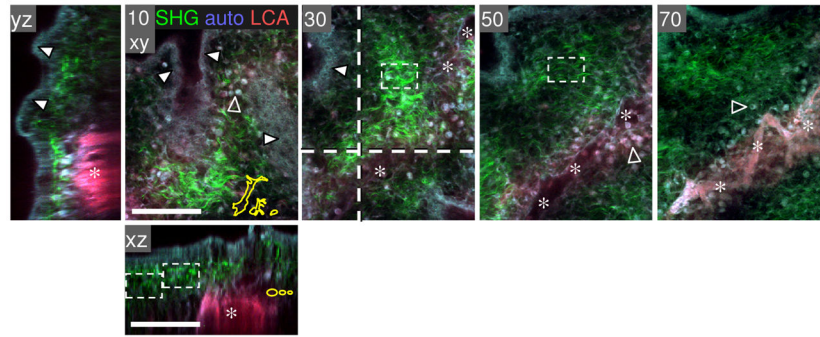
Figure 3.
Fibrillar collagen density of the chick embryo CAM. A chicken embryo (at day 12) was injected i.v. with rhodamin-conjugated lens culinaris agglutinin (LCA), and the CAM was harvested after 20 min, fixed in Zn-formalin, and analyzed by MP microscopy. Collagen fibres as detected by SHG (green), ecto/ endodermal layer of epithelial cells (white arrowheads) and blood cells (located capillary plexus or extravasated; empty arrowheads) were detected by autofluorescence signal (blue-gray); blood vessels positive for rhodamin-LCA fluorescence (red, asterisks). Image processing was performed as described in Fig. 2. Bars, 100 μm.
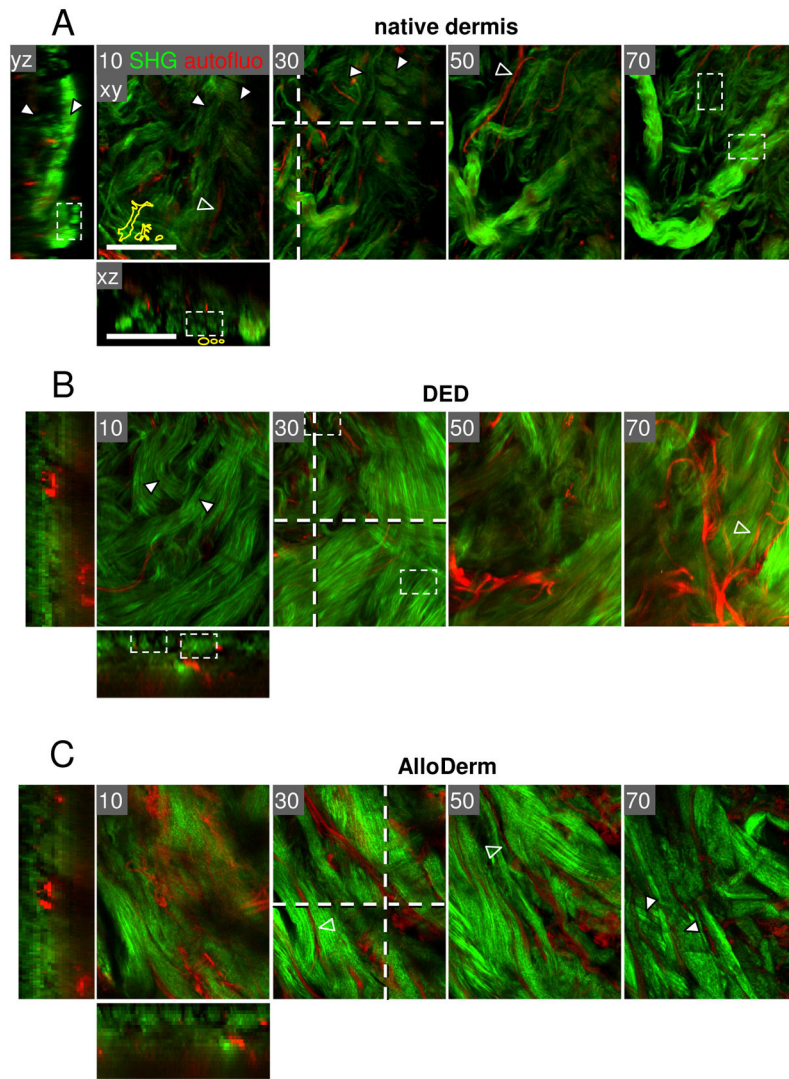
Figure 4.
Human dermis from different ex vivo sources. Two-photon-excited SHG (collagen, green) and autofluorescence (red) of 3D dermis from native back skin (A), abdomen (B), and cadaveric skin of unspecified body region (C) (AlloDerm). (A) Skin left-over from the tumor margin not needed for histopathological diagnosis was used as non-fixed whole-mount few hours post-surgery. (B) DED was obtained from abdominal skin corrections, cultivation for 2 weeks[61] and fixation by paraformaldehyde. (C) AlloDerm was used as provided by the supplier (LifeCell Corporation, Branchburg, NJ, USA) [37]. All samples were monitored from the open margin of the dermal side. Image processing was performed as described in Fig. 2. White arrowheads, collagen bundles; empty arrowheads, elastic fibres. Bars, 100 μm.
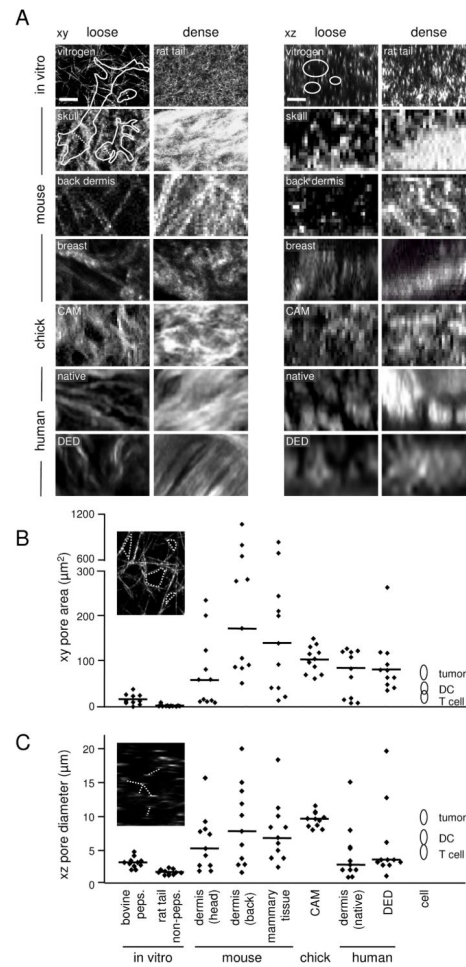
Figure 5.
Structural and quantitative comparison of collagen scaffold spacing from different models. (A) Loose and dense collagen regions obtained from selected in vitro and in vivo tissues (all derived from Fig. 1 to 4, except breast tissue). Cell outlines (from Fig. 1C) are included at 1:1 ratio in xy and xz dimension. Collagen-free gaps and pores were used for digital image analysis and quantification, using Image J. (B) Quantification of pore areas and (C) distance between fibres. Data show the medians (line) and individual measurements from different tissue regions (symbols) compared to the cross-section area and diameters of mammalian cells during migration (compare Fig. 1C). Bars, 10 µm.

Table 1

Experimental reconstitution parameters: impact on porosity of 3D collagen lattices.

Experimental condition	Pore size	Ref.
Pepsin treatment yes / no before polymerization	↑/↓	this review
low / high pH during polymerization	↑/↓	[67]
low / high temperature during polymerization	↑/↓	[68]
high / low and very high ionic strength during polymerization	↑/↓	[69]